BER the international journal of bridge engineering management and research

Seismic Safety of Aging Infrastructure: The Role of Corrosion in Vulnerability Assessment of Reinforced Concrete Bridges

Gregory Santilli Di Luia; Alberto Barontini*; Maria Giovanna Masciotta and Giuseppe Brando

Submitted: 13 August 2025 **Accepted:** 19 October 2025 **Publication date:** 10 January 2026

DOI: 10.70465/ber.v3i1.53

Abstract: The aging of road infrastructure networks, combined with the evolution of traffic loads and the tightening of regulatory requirements, demands a critical reassessment of structural safety, particularly with regard to seismic risk. Many existing bridges, designed according to outdated standards and without consideration for modern seismic criteria, are now required to meet performance levels that are significantly higher than originally intended. In this context, material degradation, especially steel bar corrosion in reinforced concrete, emerges as a critical factor that can significantly affect the structural response. This study explores feasible strategies for integrating material deterioration into seismic vulnerability assessments of critical infrastructures through numerical modelling. To this end, an existing Italian reinforced concrete bridge with Gerber saddles was analyzed as a representative case study. A corrosion evolution profile was developed to simulate realistic long-term deterioration. This approach allowed assessing the evolution of key structural parameters, including stiffness, strength, fundamental periods, and energy dissipation capacity, as well as the resulting reduction in the global safety factor, through linear and nonlinear dynamic analyses. The findings demonstrated that the progressive advancement of degradation can severely compromise seismic safety, highlighting the importance of explicitly incorporating such effects into structural assessment procedures to enhance seismic risk management of aging assets.

Author keywords: Steel corrosion; Seismic vulnerability; Bridge management; Maintenance; Concrete degradation

Introduction

In recent decades, increasing attention has been paid to the safety and durability of existing infrastructures. This growing concern is mainly due to their aging, exacerbated by a continuous rise in performance demands, while a series of recent collapses have exposed their vulnerabilities (Biondini et al.[1]), (Frangopol et al.[2]). In particular, bridges and viaducts located in earthquake-prone areas are critical components of transportation networks and play a key role in emergency response. Yet, many of these structures have already exceeded their intended service life and were originally designed according to outdated standards, often with insufficient consideration for seismic actions, structural redundancy, or material durability.

Many road bridges worldwide are currently in a critical condition. According to the 2025 Infrastructure Report Card by the American Society of Civil Engineers,[3] approximately 50% of bridges in the United States are over 50 years old, and around 9% are structurally deficient. Similar conditions can be observed in numerous other countries.

In Italy, the situation appears even more challenging: over 50% of existing infrastructures have exceeded 50 years of service life, and a significant proportion is in poor condition. The unique geographical and orographic features of Italy have resulted in a highly complex road network, requiring numerous bridges to span valleys, rivers, and man-made obstacles. According to a recent conservative estimate, the national infrastructure includes over 120,000 bridges with a span greater than 6 m, spread across an area of around 300,000 km^2 (Omar et al.[4]). When compared with the United States, this corresponds to a bridge density approximately six times higher per square kilometer in Italy (Zizi et al.[5]). At the same time, recent tragic events have brought the structural weaknesses of many Italian bridges back to the forefront. The dramatic collapse of the Polcevera viaduct in Genoa in 2018, which caused over 40 fatalities, stands as one of the most significant examples (Calvi et al.[6]), (Malomo et al.[7]).

This alarming scenario places infrastructure operators and authorities in a challenging position as they must manage a large number of assets characterized by typological and age-related heterogeneity (Salvatore et al.[8]). The tightening of technical regulations, increasing traffic loads, and exposure to more aggressive environmental conditions now require a systematic re-evaluation of the structural condition

*Corresponding Author: Alberto Barontini.
Email: alberto.barontini@unich.it
Department of Engineering and Geology, University "G. D'Annunzio" of Chieti-Pescara, Pescara, Italy

Discussion period open till six months from the publication date. Please submit separate discussion for each individual paper. This paper is a part of the Vol. 3 of the International Journal of Bridge Engineering, Management and Research (© BER), ISSN 3065-0569.

of existing infrastructures. Given that their decommissioning at the large scale is not a feasible option due to its profound social and economic consequences, safely extending the service life of these assets remains the only viable solution. However, ensuring compliance with traditional regulatory approaches for the safety assessment, both Italian and European, such as (NTC[9]), (EN 1998-2[10]), of such a large infrastructure network has become equally unsustainable, both economically and in terms of available human resources.

These critical issues have highlighted the urgent need to adopt large-scale strategies for the management and risk assessment of infrastructure assets. This approach is not entirely new, as numerous studies over the past decades have sought to develop rapid methods for more efficient infrastructure management (Grieco et al.[11]), (Saler et al.[12]). Moreover, optimized monitoring device networks and automated damage identification strategies are expected to offer essential tools for informed decision-making (Masciotta et al.[13]), (Barontini et al.[14]), (García-Macías et al.[15]). However, such procedures have not yet been systematically applied in Italy. Until recently, the main infrastructure management authorities have relied on internal protocols and evaluation criteria, which have often lacked coordination with one another.

The Italian Ministry of Infrastructure has recently issued new Guidelines for the classification and management of risk, safety assessment, and monitoring of existing bridges,[16] with the aim of introducing an advanced and common methodological framework to address these complex challenges through a structured evaluation process (ANSFISA[17]), (MIT[18]). The procedure outlined in the Italian Guidelines is a multilevel approach that enables rational and scalable management of the infrastructure assets. This is structured into three main phases, with increasing levels of detail according to the urgency and relevance of each asset (Buttarazzi et al.[19]), (Santiero et al.[20]). The initial phase of inventory and risk classification involves the application of qualitative assessment strategies across the entire infrastructure inventory. Essential data are collected, and each structure is assigned to an "attention class," reflecting its potential risk. This classification helps prioritize assets requiring more detailed investigations. The second phase of safety assessment is targeted at structures assigned to a high attention class; it includes detailed inspections, diagnostic investigations, and structural analyses to quantify the load-bearing capacity and residual safety. Finally, the third phase comprises structural monitoring. It is reserved exclusively for critical and strategically important structures. For a detailed description of each phase's main tasks, the interested reader is referred to Rossi et al.[21]. The multilevel approach responds to the necessity of optimizing economic and human resource allocation while ensuring adequate management practices for a vast, diverse, and old infrastructure network.

Within their holistic framework, the Guidelines promote the integration of material degradation processes into the assessment procedures. This requires the development of predictive models capable of estimating performance loss as a function of age, environmental conditions, and maintenance policies. Nonetheless, the Guidelines do not explicitly provide a method for incorporating degradation into vulnerability assessments through numerical simulations. This omission complicates the work of practitioners, who may lack the necessary expertise and resources to correctly implement advanced deterioration models in well-established analysis procedures.

Among the most critical degradation mechanisms of reinforced concrete structures is the corrosion of reinforcement steel bars, a time-dependent phenomenon that can significantly impair both load-bearing capacity and overall structural behavior. The reduction of the bar effective cross-sectional area, the loss of bond between steel and concrete, and the development of widespread cracking may lead to a decrease in strength, stiffness, confinement, and energy dissipation capacity, thereby altering the seismic response of the structure (Andrade et al.[22]), (Vu et al.[23]). If such phenomena are neglected or modelled in an overly simplistic manner, structural assessments may become unrealistic, ultimately resulting in an underestimation of actual risk (Cui et al.[24]). Corrosion-induced phenomena, reducing capacity and energy dissipation of reinforced concrete elements, strongly affect their seismic response (Ma et al.[25]). These phenomena may change the location of critical damage, the failure sequence, and the characteristics of the collapse mechanisms (Afsar Dizaj et al.[26]), potentially making the structural elements more brittle.

Numerous efforts have been made to model corrosion phenomena, including experimental studies investigating the deteriorating effects of corrosion on the strength and ductility of reinforced concrete sections (Almusallam[27], Idhamou et al.[28]). Numerical investigations have also been carried out to assess seismic performance following deterioration, with most studies focusing on uniform corrosion, although a few have considered localized pitting phenomena (Di Carlo et al.[29], Pinto et al.[30]). Recently, the problem of vulnerability assessment has been approached within a probabilistic framework, with increased attention given to the development of fragility functions for reinforced concrete systems under seismic conditions. Numerous studies have investigated extensive stocks of bridges across various countries, such as Italy (Borzi et al.[31]), United States (Nielson and DesRoches[32]), China (Lei et al.[33]), Greece (Moschonas et al.[34]), and Türkiye (Avsar et al.[35]), among others. These efforts have targeted different damage mechanisms and levels, employing various modelling strategies (Perdomo et al.[36], Crespi et al.[37]). Incorporating degradation processes into fragility curves is an active area of research. Studies in this field have shown that reductions in material properties due to corrosion significantly lower the seismic performance and increase the susceptibility to damage of the bridges (Cui et al.[24]). Recent developments have focused on accounting for uncertainties related to the corrosion evolution (Zhang et al.[38], Vishwanath et al.[39]), integrating multiple effects into vulnerability assessment, such as chloride ions and freeze–thaw cycles (Wang et al.[40]) or uniform corrosion and flood-induced scour (Dong et al.[41]), as well as streamlining the evaluation of seismic risk across the entire life cycle,

beginning from the construction phase (Zhong et al.[42]). In the majority of cases, existing research has concentrated on the individual structural elements scale or has addressed the problem using simplified modelling approaches. Therefore, there remains a clear need for research applying corrosion models to investigate the structural performance of real-scale bridges, particularly under the combined effects of varying stages of corrosion damage and seismic loading (Domaneschi et al.[43], Akiyama et al.[44], Akiyama et al.[45], Crespi et al.[46]).

Within this context, the present study aims to contribute to the development of robust assessment strategies that are readily implementable by practitioners and integrate time-dependent degradation scenarios. Such strategies should be capable of realistically simulating the progression of deterioration and evaluating its impact on key structural parameters. This approach improves the reliability of current well-established seismic vulnerability analysis procedures and allows for the estimation of time windows during which a structure may reach critical safety thresholds. In doing so, it promotes a shift from reactive interventions to predictive and planned maintenance strategies, which are more sustainable in the medium-to-long term. To this end, a bridge dating back to the 1960s located on a major road within the Italian national route network was selected as a representative case study. As observed on site, the bridge presents diffuse, uniform corrosion, likely induced by carbonation. Therefore, numerical models incorporating the time-dependent evolution of carbonation-induced corrosion were used to evaluate variations in dynamic properties, load-bearing capacity, and global safety factors. The results offer practical insights into the importance of accounting for degradation effects in seismic assessment models and provide replicable solutions for their integration, thereby contributing to more informed risk management strategies for vulnerable infrastructure.

The remainder of the paper is organized as follows: the second section reviews well-established corrosion degradation models developed to simulate the loss of cross-sectional area of reinforcement bars as a function of time and environmental conditions, as well as their impact on the steel and concrete mechanical properties. The third section presents the case study, detailing the bridge's geometric and structural characteristics, the numerical analyses conducted, and the degradation scenarios considered. The results of the time-dependent analyses are reported in the fourth section. Finally, the last section summarizes the main conclusions of the study.

Corrosion degradation models

Reinforcement bar corrosion is one of the main causes of degradation in reinforced concrete structures and represents a significant threat to both their durability and long-term structural safety. Under normal conditions, the bars are protected by the alkaline environment of concrete, which promotes the formation of a passive oxide film on the metal surface. This layer is stable in environments with pH > 12.5, typical of concrete. Two main mechanisms can lead to depassivation and initiate corrosion: concrete carbonation and chloride ingress. Carbonation is a chemical process affecting concrete exposed to carbon dioxide (CO_2). It involves the reaction between CO_2 and the calcium hydroxide ($Ca(OH)_2$) present in the concrete. This reaction leads to the formation of calcium carbonate ($CaCO_3$) and a significant reduction in the pH to values below 9, a condition that promotes depassivation and thereby initiates the steel corrosion process (Hussain at al.[47]). Chloride-induced corrosion, instead, is particularly severe in marine environments or where de-icing salts are used. When chloride ions reach the steel surface in sufficient concentration, they break down the passive oxide film that protects the steel, even when the pH remains high (Tuutti et al.[18]).

The corrosion compromises the bond between steel and concrete, reduces the load-bearing cross-section of the reinforcement, and leads to the formation of cracks and spalling of the concrete (Imperatore et al.[48]). These phenomena arise from various forms of deterioration (Coronelli & Gambarova[49], Meda et al.[50]; Guo et al.[51]; Yang et al.[52]), including a reduction in the ultimate concrete strength within the cover and parts of the confined core, as well as a loss of confinement effectiveness provided by transverse reinforcement bars. Leading to a reduction in the cross-sectional area of both longitudinal and transverse steel bars, corrosion increases the risk of bar buckling due to combined section loss and reduced confinement, and lowers the yield strength, ultimate strain, and ductility of the steel. The reduction in stirrup confinement caused by corrosion is among the main factors contributing to the loss of seismic performance (Xu et al.[53] and Di Mucci et al.[54]). All these effects result in a significant reduction in the service life of the degraded system and an increase in its seismic vulnerability (Di Sarno & Pugliese[55]). The inclusion of these degradation mechanisms in the vulnerability assessment is essential for a correct evaluation of the structural performance over time, but requires the definition of sound modelling strategies that are described in the following sections.

Corrosion evolution rate

The well-established conceptual framework developed by Tuutti et al.[18] has demonstrated effective in modelling corrosion evolution profile. This model divides the corrosion process in reinforced concrete into two distinct phases: (i) the initiation phase, during which aggressive agents such as carbon dioxide (in the case of carbonation) or chloride ions (in chloride attack scenarios) penetrate the concrete cover and gradually reach the depth of the embedded reinforcement; and (ii) the propagation phase, which begins once the passive layer, which protects the steel in the alkaline environment, is destroyed.

Carbonation progresses over time, moving inward from the exposed surface. The carbonation depth can be described by a parabolic law, as proposed by Tuutti et al.[18], which relates the depth to the square root of exposure time, reflecting the diffusion-controlled nature of the process:

$$x(t) = K_c \cdot \sqrt{t} \tag{1}$$

where x represents the thickness of the carbonated layer in millimeters, K_c is the carbonation rate coefficient, and t denotes the time in years. Building on this general formulation, several modifications have been proposed to ensure a sound estimation of the carbonation rate coefficient. One well-established solution, identified through a comparison of existing models in the DuraCrete Report,[56] is the following:

$$x(t) = \sqrt{\frac{2k_1k_2D_{eff}C_s}{a}} \cdot \left(\frac{t_0}{t}\right)^n \cdot \sqrt{t} \tag{2}$$

where D_{eff} is the effective diffusion coefficient at defined compaction curing end environmental conditions, k_1 and k_2 are constant parameters accounting for the influence of workmanship and environmental exposure, respectively, a is a binding capacity for CO_2, t is the time in service, and t_0 is the reference period. However, various models have been developed to predict carbonation depth, yet there remains no consensus on how to estimate the carbonation coefficient (Silva et al.[57]), as it depends on several factors that are not always easy to determine under real exposure conditions. As an alternative to models that require multiple parameters to describe the factors influencing the diffusion of carbon dioxide into concrete, characteristic values of the carbonation rate coefficient, based on specific concrete qualities and exposure conditions, may be used for a first-level assessment. A more detailed discussion of experimentally estimated values and carbonation prediction models can be found in Hills et al.[58] and Silva et al.[57]

Irrespective of the adopted formulation for K_c, the initiation time, required for carbonation to reach the reinforcement level, namely the concrete cover depth x_{cover}, can be derived by inverting Eq. (1):

$$t = \left(\frac{x_{cover}}{K_c}\right)^2 \tag{3}$$

This formulation is widely adopted in technical standards and guidelines, such as fib Bulletin 34,[59] and serves as a fundamental tool for service life assessment of reinforced concrete structures.

Unlike carbonation-induced corrosion, chloride attack can initiate localized corrosion (pitting) even under alkaline conditions, leading to rapid and severe cross-sectional loss in the affected areas. The transport of chlorides through the concrete cover can be modelled using Fick's second law of diffusion, which provides a framework for predicting the penetration depth and concentration profile of chlorides as a function of time and material properties (Tuutti et al.[18]).

$$\frac{\partial C}{\partial t} = \frac{\partial}{\partial t}\left[D(x,t)\frac{\partial C}{\partial t}\right] \tag{4}$$

where C denotes the chloride concentration, D is the diffusion coefficient, x represents the distance from the external surface at which the chloride concentration is measured in millimeters, and t denotes time in years. If the surface chloride content C_S, and the diffusion coefficient D, remain constant over time, the chloride concentration at a given x and at time t is given by:

$$C(x,t) = C_s\left[1 - erf\left(\frac{x}{2\cdot\sqrt{D_{app}\cdot t}}\right)\right], C_s = C(x=0,t) \tag{5}$$

where D_{app} is the apparent diffusion coefficient [m^2/s] and erf represents the Gaussian error function. The diffusion of chlorides in concrete has been extensively studied due to its significant role in determining the time required for chloride ions to reach the reinforcement and initiate corrosion. An effective empirical approach for modelling chloride penetration is presented in the DuraCrete Report.[56] For recent models addressing corrosion initiation and propagation, the interested reader is referred to Cui et al.[24] and Kim et al.[60]

For the vulnerability assessment of the specific case study presented in this work, only carbonation-induced corrosion is considered, based on the evidence collected on site regarding the degradation affecting the bridge. Therefore, chloride propagation models are not discussed further.

Corrosion model for bars

During the propagation phase of corrosion, electrochemical reactions induce a mass loss in the reinforcement bar reflected in the progressive reduction of its effective cross-sectional area. The residual area $\Delta s(t)$ at time t can be quantitatively assessed through the approach proposed by Saetta et al.[61] This model accounts for both the pace of the corrosion process and its mechanical consequences on the steel, providing a time-dependent estimate of reinforcement degradation consistent with actual environmental exposure conditions:

$$\Delta_s(t) = \frac{N_s\cdot\pi\cdot[\varnothing_0 - n\cdot\varnothing'(t)]^2}{4}, t > t_0 \tag{6}$$

where N_s is the number of reinforcement bars, $\emptyset_0$ is their initial diameter, $\emptyset'(t)$ is the corrosion penetration depth, t_0 is the corrosion initiation time, and the coefficient n accounts for the possibility of either one-sided or two-sided corrosion attack on the reinforcement. The corrosion penetration depth can be evaluated as follows:

$$\varnothing'(t) = 0.0116\cdot i_{corr}\cdot(t - t_0) \tag{7}$$

where the constant 0.0116 is a conversion factor to switch from $\mu A/cm^2$ to $mm/year$ and i_{corr} is the corrosion rate, calculated according to Vu et al.[23] as a function of the concrete cover depth x_{cover}, and the water to cement *ratio a/c*:

$$i_{corr} = \frac{37.8\cdot\left(1 - \frac{a}{c}\right)^{-1.64}}{x_{cover}} \tag{8}$$

Steel bar corrosion significantly affects both the strength and ductility of the reinforced concrete element. The ultimate deformation of corroded bars decreases as corrosion increases. Experimental studies have identified an exponential decay of the ductility (Imperatore et al.[48]):

$$\varepsilon_{su}^{corr} = \varepsilon_{su}e^{-0.055CR[\%]} \tag{9}$$

Table 1. Empirical coefficients for reduced steel yielding stress

Reference	Type of corrosion	CR[%]	β_s
Imperatore et al.[15]	Pitting	–	0.0199
	Uniform	–	0.0151
Wang and Liu[62]	Pitting	–	0.0198
	Uniform	–	0.0124
Du et al.[24]	–	0–18	0.0050
Lee et al.[63]	–	0–25	0.0120
Morinaga[64]	–	0–25	0.0170
Zhang et al.[65]	–	0–67	0.0100
Clark et al.[66]	–	0–28	0.0130

where ε_{su}^{corr} and ε_{su} are the ultimate strain with and without corrosion, respectively, and CR[%] refers to the percentage of corroded mass, corresponding to the sum of the initial mass before corrosion M_0 and the ratio of the post-corrosion mass M_C to the initial mass: $M_0 + M_C/M_0$.

Similarly, experimental studies have demonstrated that the yield strength tends to decrease as a function of the mass loss induced by the corrosion process, the type of corrosion (either uniform or localized pitting), and the environmental exposure conditions. The corroded yield stress f_y^* can be expressed by the following equation (Di Sarno et al.[55]):

$$f_y^* = (1 - \beta_s CR[\%]) \cdot f_y \tag{10}$$

where f_y denotes the uncorroded yield stress and β_s is an experimental coefficient, which depends on whether the reinforcement is exposed to the environment or embedded within the concrete, as well as on the type of exposure.

Table 1 summarizes the main empirical coefficients proposed in the literature for modelling the loss of capacity of reinforcement steel bars subjected to corrosion. In most studies, the results refer to specific ranges of CR[%], reported in Table 1, but without specifying whether uniform or pitting corrosion is occurring. This introduces uncertainties regarding the applicability of the models. In contrast, the studies conducted by Wang et al.[62] and Imperatore et al.[48] stand out for having provided separate coefficients for the corrosion types, although the range of CR[%] is not explicitly reported.

Corrosion model for concrete

The presence of cracking caused by the expansive pressure of corrosion products, combined with the loss of bond strength between steel and concrete, significantly compromises the load-bearing capacity of the section and the interaction between materials. Numerous experimental studies (Ghanooni et al.[67]), (Imperatore et al.[68]) have highlighted a progressive reduction in the compressive strength, elastic modulus, and hardness of concrete as corrosion-induced damage advances.

The degradation of concrete mechanical properties may be successfully modelled using the formulation proposed by Coronelli et al.[49]. The reduced concrete strength f_c can be evaluated as follows:

$$f_c = \frac{f_{c0}}{1 + K\frac{\varepsilon_1}{\varepsilon_{c0}}} \tag{11}$$

In Eq. (12), f_{c0} is the undegraded concrete strength, K is a coefficient related to bar diameter and roughness (equal to 0.1 for medium-diameter ribbed bars), ε_{c0} is the strain at peak stress in compression, and ε_1 is an average value of the tensile strain in cracked concrete at right angles to the direction of the applied stress, which can be evaluated by means of the following relationship:

$$\varepsilon_1 = \frac{b_f - b_i}{b_i} = \frac{N_s w}{b_i} \tag{12}$$

where b_i is the width of the unaltered concrete cross-section and b_f is the width after corrosion cracking, accounting for the number of steel bars, N_s, and the mean crack opening for each bar, w. Among the relationships proposed in literature to evaluate the total crack opening w for a given corrosion level, the relation proposed by Molina et al.[69] may be used:

$$w = \sum u_{icorr} = 2\pi\,(v_{rs} - 1)\,x \tag{13}$$

Here v_{rs} is the ratio of volumetric expansion of the oxides with respect to the virgin material, x is the depth of the corrosion attack, and u_{icorr} is the opening of each single corrosion crack. The value of v_{rs} can be assumed to be 2, as observed by Molina et al.[69].

The alteration of concrete elastic modulus due to corrosion may be modelled as a function of the varying compressive strength; for example, in accordance with the Italian standard (NTC[9]).

Application to the Case Study

The case study under analysis is a viaduct located on the "S.S. 16 Adriatica," a main road in the Italian national route network. It was selected from a group of assets used to implement and test the evaluation framework envisaged by the new Italian Guidelines for the safety management

of existing bridges. Moreover, the peculiar aspects of the viaduct, including a heavy intervention on the piers and widespread degradation, make it a relevant testbed for advanced assessment strategies, which account for the evolution of corrosion over time and its consequent impact on the structural response.

Bridge description

The bridge, shown in Fig. 1a, was constructed between 1961 and 1980, likely following a design predating 1960 and therefore lacking any reference to seismic standards for constructions. The deck has a total length of 84 meters, divided into five spans: two end spans of 15.40 meters each and three intermediate spans of 17.55 meters. The entire structure is made of ordinary reinforced concrete.

Each span comprises five main girders (Fig. 1b, 1c) with a segmental arch geometry, rectangular in section, approximately 0.35 meters wide and varying in height from 2.22 meters at the supports to 1.14 meters at mid-span. The main girders are connected by transverse crossbeams and a reinforced concrete slab. The continuity of the roadway is maintained by reinforced rubber expansion joints at the Gerber saddles and abutments. The Gerber saddles are equipped with unidirectional support devices consisting of steel bearings. These are composed of a cylindrical steel roller inserted between two steel plates, allowing relative movement through rolling. The abutments are monolithic and feature front and wing walls, guard curbs, and a bearing platform without bridge bearings.

The piers (Fig. 1d) range in height from 6.90 meters (end piers) to 9.30 meters (central piers) and consist of frames composed of five rectangular columns tapered toward the top and connected by two levels of stiffening crossbeams, one at the top and one approximately 4.00 meters below the underside of the deck.

The five columns composing the piers present solid rectangular cross-sections, with dimensions that vary alternatively between 85 × 35 cm (even columns) and 115 × 65 cm (odd columns). The measured concrete cover is 3 cm. In the absence of original design drawings, the reinforcement layout was reconstructed through a simulated design, which suggested the presence of longitudinal reinforcement bars with a diameter of 26 mm and stirrups with a diameter of 12 mm spaced at 10-cm intervals. The consistency of these details was also confirmed through visual inspection in areas where the concrete cover is missing.

As for the reinforcement steel, AQ50 grade was assumed, as it was commonly used at the time of construction. This type of steel is characterized by a Young's modulus, E_s, equal to 200 GPa, a yield strength, f_y, of 270 MPa and an ultimate strength, f_u, of 545 MPa. For the concrete, C16/20 class was adopted, based on the results of a series of core sample tests previously carried out on the structure and reported in technical documents, which indicate a material already affected by degradation. The same characterization approach was applied to the other structural elements, such as the deck beams; however, in the present study, these components are given less emphasis, as the primary objective is the assessment of the seismic response of the structure, which is predominantly governed by the behavior of the piers.

Since the early 2000s, inspection reports have documented a complex degradation state, combining superficial and advanced phenomena. Extensive biological colonization and signs of persistent moisture, including vertical staining consistent with uncontrolled infiltration or run-off, were observed mainly on the deck and abutments (Fig. 2a, 2b), with little or no evidence on the piers. These conditions promoted the disintegration of the cementitious matrix and a local reduction in surface alkalinity, particularly on the abutments and at the Gerber saddles (Fig. 2b, 2c). In addition, there was advanced carbonation of the concrete in many areas. In more critical sections, specifically at the base of the pier shafts, large portions of the concrete cover had spalled, exposing the reinforcement bars (Fig. 2d–2f). The steel exhibited signs of active corrosion, including oxidation and localized loss of cross-sectional area. The poor quality of the concrete, characterized by high porosity and an uneven aggregate distribution as identified on-site, along with the sporadic presence of de-icing salts percolating through the structural elements, likely contributed to the accelerated corrosion process.

Between 2016 and 2017, due to the advanced state of deterioration observed in many of the structural elements, a programme of extraordinary maintenance was initiated, aimed at the structural repair of the abutments, piers, underside of the deck, slab, and Gerber saddles. The project also included the replacement of road safety barriers and the refurbishment of the deck drainage system. Due to financial constraints, the interventions were only partially completed, and some of those carried out were not executed in full compliance with best construction practices. Among the completed works, pier jacketing was carried out. For each pier, only the two outer shafts and the central one were jacketed (Fig. 2a). Given the suboptimal execution of some maintenance works, the actual effectiveness of the jacketing has been investigated in Section 4. Moreover, recent inspections have revealed evidence of the continued progression of corrosion.

The structure, in its actual configuration, was assessed in accordance with the Italian Guidelines for the safety management of existing bridges. Specifically, the methodologies included in the first phase of the classification process, described in the introduction section, were applied. These involved data collection, visual inspection, and a simplified preliminary analysis of the structural behavior. Following this assessment, the bridge was classified as belonging to the "High Attention Class," a category that requires a detailed evaluation phase. This second phase involves advanced structural analysis using numerical models and is aligned with the performance-based criteria defined by current standards.

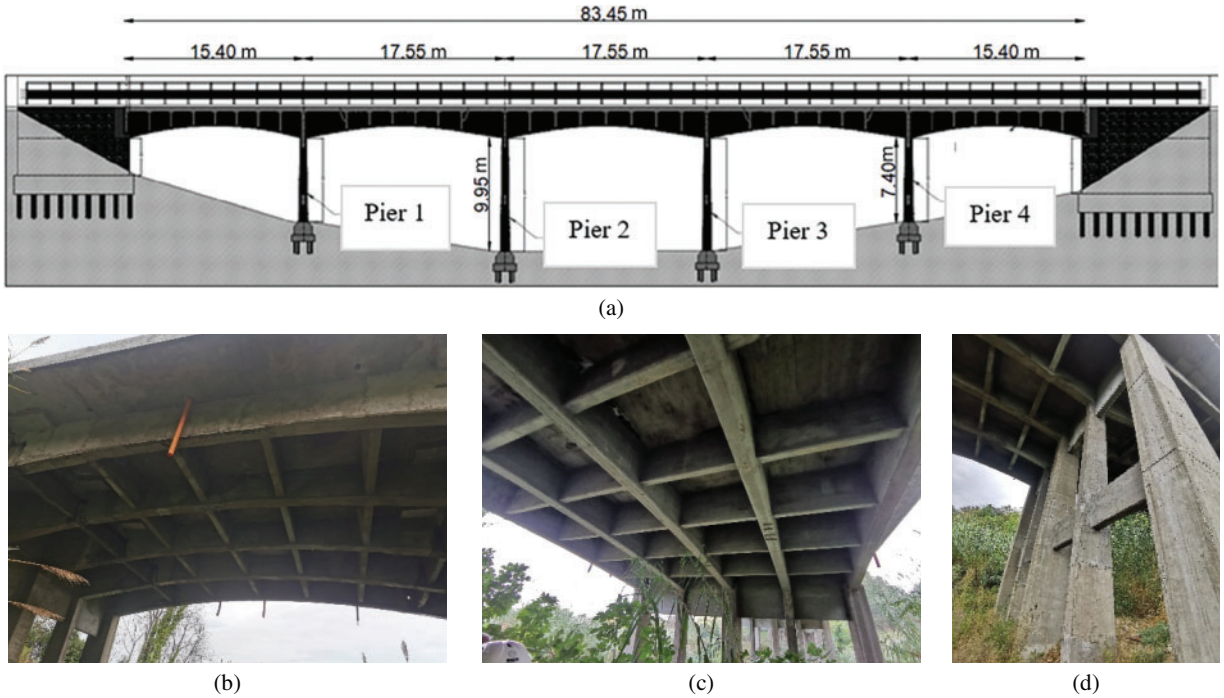

(a)

(b) (c) (d)

Figure 1. Investigated bridge: (a) schematic elevation; (b) view of span 3 with the two central piers; (c) view of span 5 deck; and (d) view of a central pier

(a) (b) (c)

(d) (e) (f)

Figure 2. Observed degradation: (a) bridge deck; (b) abutment; (c) Gerber saddle; (d) pier 4; (e) pier 2; and (f) pier 3

Model description and numerical analyses

The numerical model was developed using Midas Civil software[70] (Fig. 3a) with the objective of accurately reproducing the structural behavior of the bridge.

The model included all main structural elements, such as the piers, deck beams, slab, and Gerber saddles. The finite elements used in the model include both beam and plate elements. One-dimensional (1D) Timoshenko beam elements characterized by a total of 12 degrees of freedom were used to model the pier shafts, the deck girders, and the crossbeams. Two-dimensional (2D) Mindlin–Reissner plate elements, combining membrane with plate behavior were

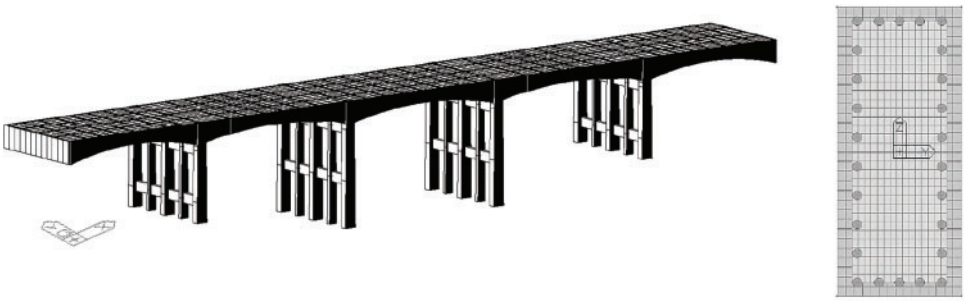

(a) (b)

Figure 3. Numerical model: (a) axonometric view and (b) detail of the subdivision in fibers of a pier shaft section

Table 2. Properties of the concrete and rebar steel in undegraded condition

Rebar steel (AQ50)			Concrete (related class C16/20)	
E_s [Mpa]	f_y [MPa]	f_u [MPa]	E_c [MPa]	f_{cd} [MPa]
200000	270	545	28820	9.41

Table 3. Mechanical parameters for confined and unconfined concrete and steel

Park et al.[71]				Menegotto and Pinto[28]		
Parameter	Unit	Unconfined	Confined	Parameter	Unit	
K	[-]	1.00	1.062	fy	[MPa]	270
fc	[MPa]	9.41	9.41	E	[MPa]	200000
ε_{c0}	[%]	0.0020	0.0021	b	[-]	0.0052
ε_{c1}	[%]	0.0034	0.0067			
ε_{cu}	[%]	0.0035	0.0077			

adopted to model the deck slab. The mesh was generated as a regular square grid, with each element having 24 degrees of freedom. The piers were modelled as fixed at the base, while elastic links were introduced at the Gerber saddles to simulate the behavior of the bearings and reproduce the actual kinematic response of the structure. To simulate the nonlinear behavior, advanced constitutive laws were adopted, namely, the approach proposed by Park et al.[71] for concrete and by Menegotto and Pinto[72] for steel. The cross-sections were discretized using a fiber approach (Fig. 3b) into uniaxial fibers of concrete and steel, each characterized by its own stress–strain constitutive law and contributing to the response only through axial deformation. Integration of the individual fiber responses made it possible to reconstruct the global force-deformation behavior of the element, using the flexibility-based beam–column formulation (Taucer et al.[73]), recognized for its ability to simulate the spread of plasticity along the length of the element. The mechanical properties adopted in the model for both concrete and steel are reported in Tables 2 and 3.

In particular, Table 3 also reports the coefficients associated with the strain hardening ratio of the steel (b) and the strength increase of the concrete due to confinement (K). The parameters indicated in Table 3 correspond to time 0, that is, to the absence of corrosion. For a pier subjected to seismic action, a good level of confinement increases both the strength and ultimate deformation of the element, thereby allowing a greater energy dissipation, as discussed by Xu et al.[53] and Di Mucci et al.[54]

Several analyses were carried out to assess the structural response under service conditions and in the presence of seismic actions. An initial linear static analysis was conducted to estimate the structural response to permanent and traffic loads. Then, focusing on the seismic vulnerability assessment, a linear dynamic analysis was first performed using the response spectrum method. This represents a standard approach widely adopted in professional practice for the assessment of structural seismic response. Therefore, integrating degradation effects within this method was a crucial step toward enhancing conventional assessment procedures. In this case, a behavior factor q of 1.5 was adopted, in accordance with the regulatory provisions, to account for a partial energy dissipation capacity of the structure while maintaining an essentially elastic approach. The analysis provided the seismic demand, which was subsequently compared with the capacity evaluated according to the current

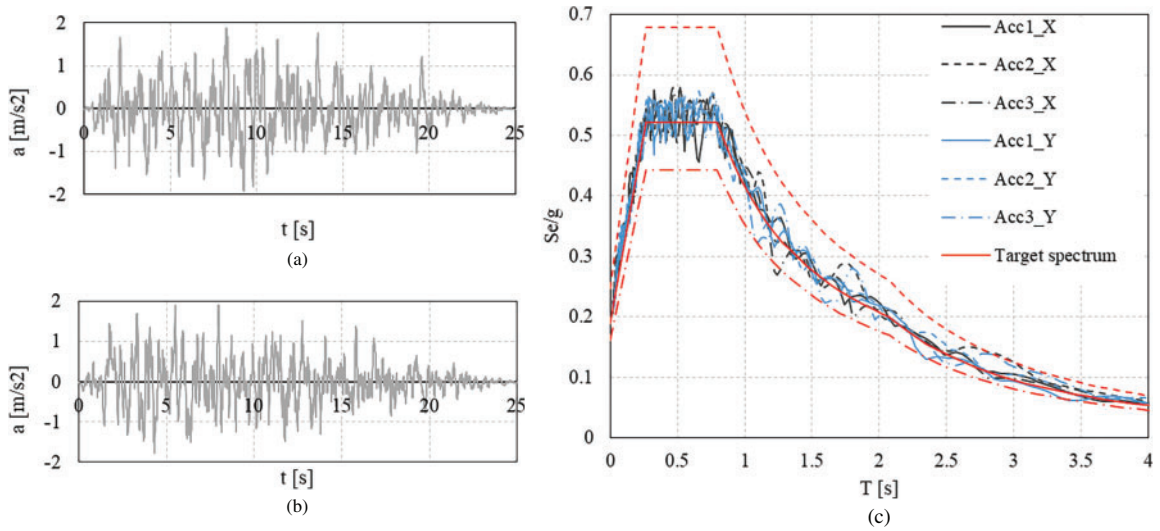

Figure 4. Nonlinear dynamic analysis input: (a) x-direction accelerogram, set 1, (b) y-direction accelerogram, set 1, and (c) spectrum compatibility verification

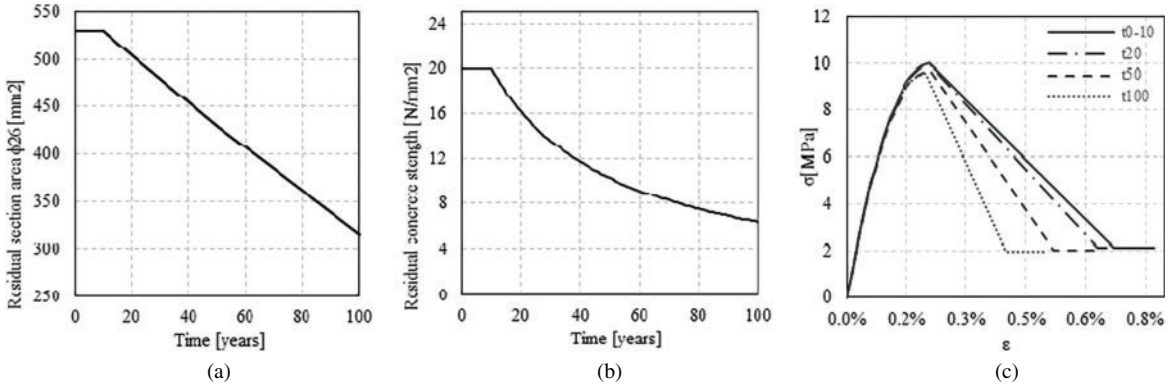

Figure 5. Time evolution: (a) reinforcement cross-sectional area; (b) concrete compressive strength; (c) Park et al.[71] model, variation of the constitutive law as the degradation of the stirrups increases

Italian technical standards (NTC[9]). To this end, concrete was described using a uniaxial parabola–rectangle law, while steel was modelled with an elastic–perfectly plastic model.

For a more rigorous assessment of degradation effects, and a detailed investigation of variations in ductility and energy dissipation, a nonlinear dynamic analysis was also performed. To this end, nine artificial accelerograms compatible with the design spectrum at the bridge site as specified by the Italian standard (NTC[9]), organized into three sets of records corresponding to the *x*-, *y*-, and *z*-direction (Fig. 4), were generated, taking the maximum effect they produced on the structure. In the analyses, the considered permanent loads included the self-weight of the structure, deck slab, asphalt, and safety barriers (guard-rails). For the modelled elements, the self-weight was automatically calculated by the software, based on geometry and material properties; for the non-modelled elements, permanent loads were introduced as linear or distributed loads. Variable loads and traffic loads were neglected in the dynamic analyses, in accordance with the provisions for seismic verifications prescribed by the Italian standard (NTC[9]).

Corrosion scenario

The case study was considered as subjected to a uniform corrosion induced by carbonation. The time evolution of the mechanical parameters was calculated according to the formulations reported in the "corrosion degradation model" section. More specifically, the first step involved the estimation of the time required for the carbonation to reach the stirrups and subsequently the longitudinal reinforcement bars, using Eq. (3). For low-quality concrete with a water-cement ratio of 0.6, typical value for infrastructure built before the 1980s, a carbonation rate coefficient equal to 10 is adopted (Fellitti et al.[74]). Using Eq. (7), the loss of reinforcement cross-section over time was determined. A corrosion rate of approximately 5.2 μA/cm^2 was determined corresponding to a penetration progress of 0.06 mm/year. Eq. (11) was then used to evaluate the residual yield strength as a function of the corroded mass. Finally, Eq. (12) was applied to calculate the reduction in concrete compressive strength and modulus of elasticity as a function of the same.

Fig. 5a and 5b illustrates the progressive reduction of both the cross-sectional area of the reinforcement bars and

Table 4. Reduction in steel and concrete properties with progressing corrosion

	Steel properties				Concrete properties	
	Longitudinal reinforcement		Transverse reinforcement			
Time [years]	A_s[mm^2 (%)]	f_y[MPa (%)]	As[mm^2 (%)]	f_y[MPa (%)]	R_{ck}[MPa (%)]	E_c[MPa (%)]
0	530.93 (0)	270 (0)	113.1 (0)	270 (0)	30 (0)	31447 (0)
10	530.93 (0)	270 (0)	113.1 (0)	270 (0)	30 (0)	31447 (0)
20	504.39 (−5)	268.88 (−0.4)	101.03 (−10.4)	269.50 (−0.2)	24.28 (−19)	30010 (−4.6)
50	428.93 (−19)	266.02 (−1.5)	65.95 (−41.7)	268.25 (−0.6)	15.44 (−49)	27227 (−13.4)
100	316.95 (−40)	261.75 (−3.1)	29.12 (−74.3)	266.63 (−1.2)	9.61 (−68)	25322 (−19.5)

the concrete compressive strength. In the case study under consideration, the corrosion process is assumed to begin in the tenth year of the structure service life, coinciding with the point at which the carbonation depth exceeds the concrete cover thickness. Furthermore, the reduction in concrete compressive strength is considered to develop progressively following the onset of corrosion. For the sake of completeness, Fig. 5c shows how the constitutive law of confined concrete varies according to the Park et al.[67] model as the corrosion of the stirrups increases.

The analyses presented in the following sections consider both the initial, undegraded configuration of the structure and several degraded conditions corresponding to 10, 20, 50, and 100 years of service. At each time step, the model is updated to present the residual cross-section of the reinforcement as well as the reduced strength of steel and concrete. This timeframe allows for an evaluation of the structural response over time, encompassing both the current age of the bridge under study, now exceeding 50 years, and the typical design service life of such structures, generally assumed to be 100 years. Tables 4 reports the evolution of the mechanical and geometrical parameters affected by corrosion, for steel and concrete respectively.

The reported values clearly show that, as expected, corrosion has a significant impact on the steel, particularly on its cross-sectional area. The area of the stirrups undergoes a more rapid and drastic reduction compared to the longitudinal reinforcement, although the reduction for the latter is still significant. This is a crucial finding, as the reduction in the area of the stirrups compromises the confinement effect and the shear strength. Regarding the yield strength, the reduction occurs much more slowly, suggesting that the primary effect of corrosion is the loss of cross-section rather than a rapid alteration of the mechanical properties. Regarding the concrete, it is observed that the compressive strength undergoes a significant reduction, reaching a 68% decrease after 100 years. Concurrently, the elastic modulus, determined as a function of the varying compressive strength, also decreases, although to a less pronounced extent.

Considering that the piers play the most significant role in the bridge's seismic performance, and that on-site inspections revealed a lower extent of corrosion in the deck and beams, the aforementioned corrosion models have been applied only to the piers in the numerical analyses.

Due to the absence of precise measurements of rebar diameter loss and repair works conducted over time to restore the concrete cover, a quantitative validation of the corrosion models is not feasible. However, the visible degradation documented since the early 2000s, when the bridge was approximately 30 years old, and the evidence observed in unrestored areas qualitatively confirm that the corrosion process had significantly progressed and is still ongoing.

Results

The main results of the analyses discussed in the previous section are hereafter presented. As the primary objective of these analyses is to evaluate the impact of degradation on the structural response and to observe how this evolves over time due to corrosion, results from the detailed assessment according to the Italian guidelines, which focuses on the structure in the undegraded condition, are included as a reference.

Influence of degradation on vibration modes

The effect of corrosion was first investigated through eigenvalue analyses, carried out by progressively varying the mechanical parameters of the materials to simulate the evolution of structural degradation over time, as described in the previous section, from the initial condition (t_0) up to 100 years (t_{100}). Fig. 6 shows the mode shapes associated with the first three vibration modes in the initial configuration, while Fig. 7 illustrates the evolution of the corresponding natural periods over time (expressed in years).

Mode shapes and participating masses resulted only marginally affected by corrosion, likely due to the homogeneous and widespread nature of degradation in the examined scenarios. However, a clear correlation was observed between material deterioration and the increase in natural periods, indicating a progressive loss of stiffness. In particular, the first mode of vibration, typically associated with the global behavior of the structure, exhibited the most significant variation, with a period increase of 6.5%, whereas the periods associated with the second and third

(a) (b) (c)

Figure 6. Bridge mode shapes: (a) first mode; (b) second mode; and (c) third mode

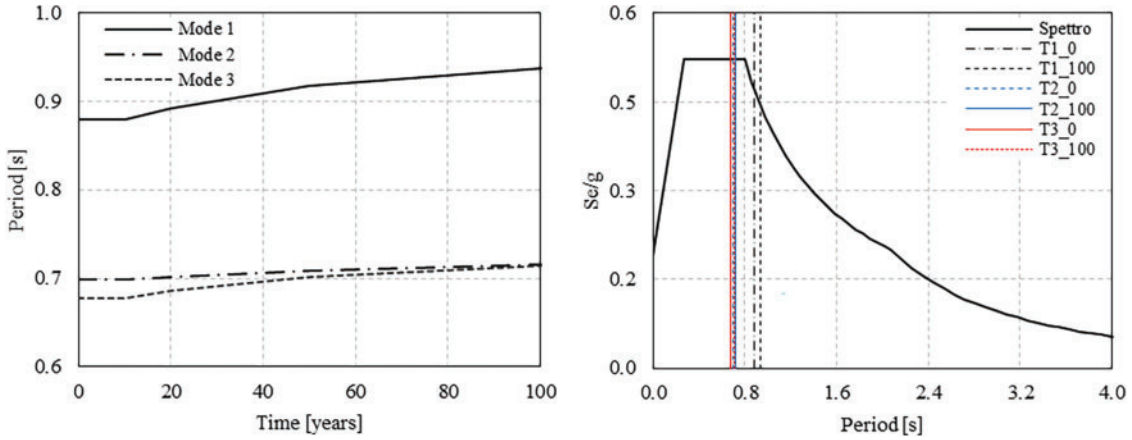

(a) (b)

Figure 7. (a) Variation of the natural periods with increasing degradation and (b) variation of the spectral acceleration with increasing degradation

modes showed more limited upshifts. Interestingly, advanced corrosion states led to an inversion of the order between second and third modes. In Fig. 7b, we can observe how the minimal reduction in stiffness has a negligible effect on the spectral acceleration of modes 2 and 3, which are located on the plateau of the spectrum. Conversely, for mode 1, which falls within the descending branch of the spectrum, the same loss of stiffness causes a decrease in the spectral acceleration.

The most significant increase was observed in the early years, with the growth rate slowing after approximately 50 years, indicating a nonlinear relationship between the progression of degradation and the variation in the dynamic properties of the structure.

Influence of degradation on structural capacity

The comparison between the demand (Fig. 8) and structural capacity shows that the bridge is inadequate from both a static and seismic perspective, even without taking into account the effects of degradation. The increased design loads required by current regulations, particularly those related to traffic, revealed that the deck beams fail to meet the criteria for both bending and shear, having originally been designed for significantly lower loads.

A similar outcome emerged from the seismic assessment: as the structure was not originally designed to withstand seismic forces, the piers exhibit structural deficiencies and fail the checks for combined compression and bending. In summary, for the relevant load combinations, the structure demonstrated a static safety factor of 0.4 and a seismic safety factor of 0.37.

The influence of degradation on the structural capacity, specifically in terms of shear and flexural resistance as well as maximum displacement, was investigated through the linear dynamic analysis using the response spectrum method. Fig. 9 shows the time evolution of shear capacity, V_{Rd}, and shear demand for the four piers in the two principal directions. The capacity is identical for all piers, as they possess equivalent geometric, structural, and mechanical characteristics.

While the shear capacity of the section progressively decreases over time due to degradation phenomena, the shear demand on each individual pier remains almost constant. This reflects in the evolution of the safety factors, reported in Fig. 10. In particular, after 50 years, the safety factor in the x-direction for Piers 1 and 4 reduces below 1. As corrosion further progresses over time, the same outcome occurs for the remaining piers. In the y-direction, by contrast, the initially small safety margin for Piers 2 and 3 is exceeded shortly after the onset of corrosion. The other piers remain verified until approximately 40 years.

To assess the influence of corrosion on bending capacity, the shafts of the most heavily loaded pier were considered and bending moment–axial compression interaction domains were produced. Fig. 11 presents the interaction domains for the two types of sections of the shafts forming the pier, namely, 85×35 cm^2 and 115×65 cm^2.

As corrosion progresses, the interaction domains undergo large reductions. The shafts with the original cross-section (85×35 cm^2) remain compliant in the y-direction even beyond 100 years, while they fail to meet the requirements in the x-direction shortly before 100 years. However, the

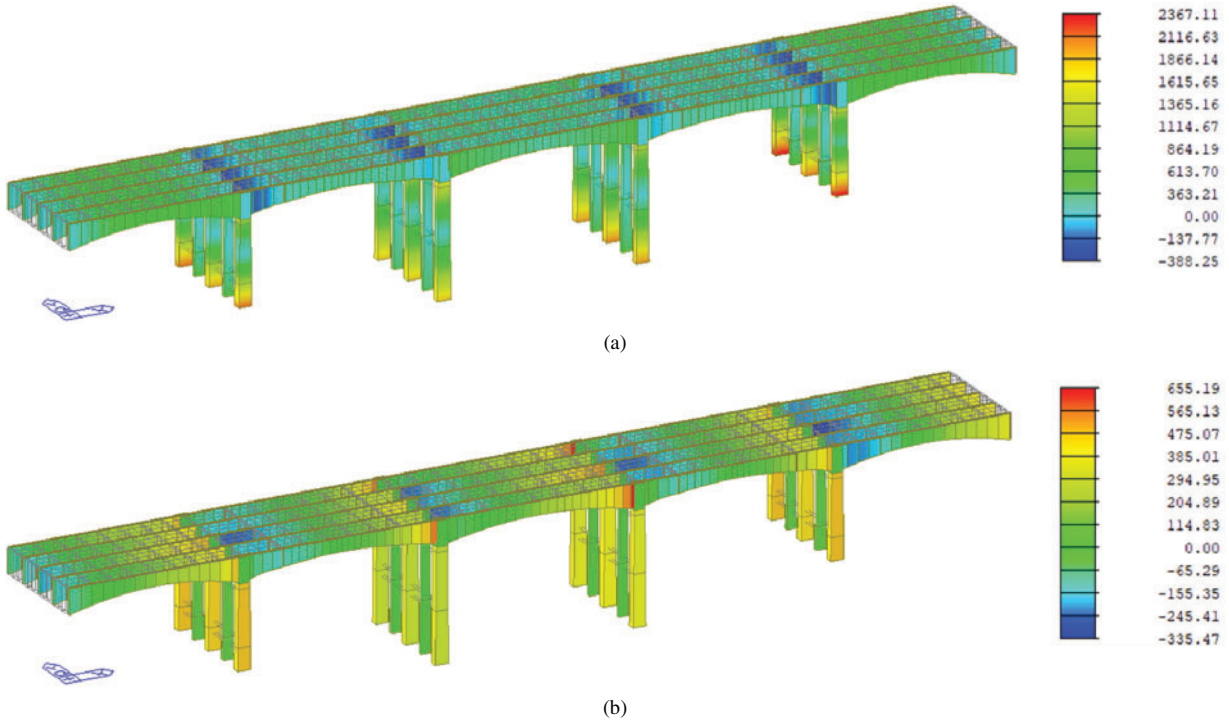

Figure 8. Maximum envelope of forces for seismic combinations: (a) bending moment, x-direction [kNm] and (b) shear, x-direction [kN]

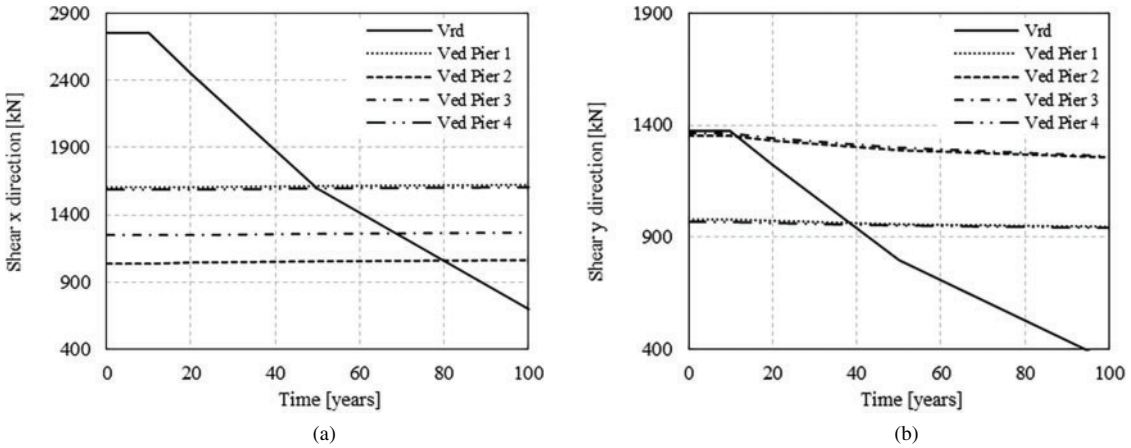

Figure 9. Effects of degradation over time: (a) variation of applied and resistant shear, x-direction and (b) variation of applied and resistant shear, y-direction

higher safety margin of the original cross-section is primarily due to a significantly lower demand, as the enlarged shafts, with a 115 × 35 cm^2 cross-section resulting from the strengthening intervention, absorb most of the seismic actions. Therefore, the enlarged shafts, being subjected to higher demands, present an insufficient capacity even in the reference undegraded condition.

The progression of corrosion also affects deformations. Fig. 12 shows the increase of the displacement at the top of the piers in the *y*-direction, transverse to the deck, under seismic action, with increasing degradation, as estimated through the linear dynamic analysis. As expected, displacement growth is more pronounced in the central piers, which are located further from the end abutments, with increases of approximately 2%, 4.5%, and 7% after 20, 50, and 100 years, respectively.

Influence of degradation on the ductility and dissipative capacity

The effects of progressing corrosion on ductility and energy dissipation capacity were investigated through nonlinear dynamic analysis. The three sets of artificial accelerograms,

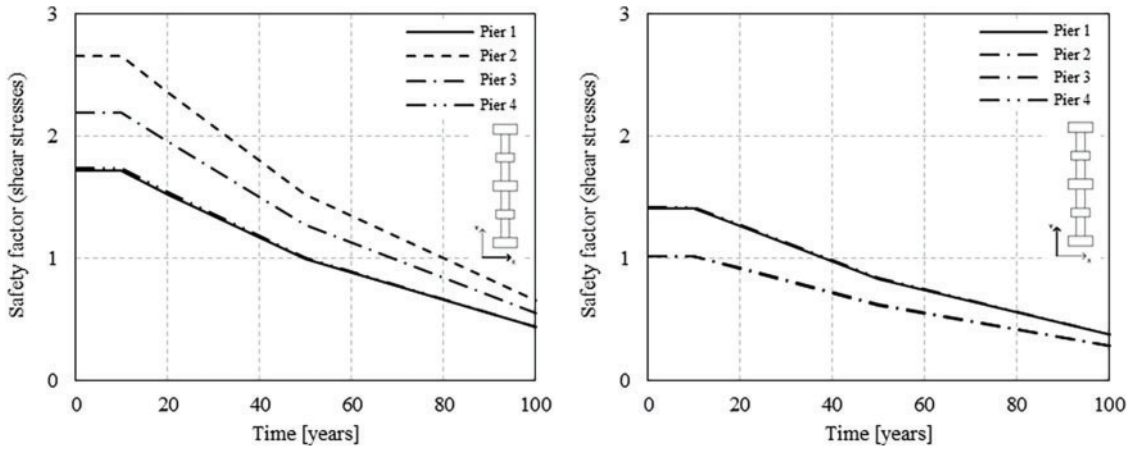

Figure 10. Variation of shear safety factor over time: (a) x-direction and (b) y-direction

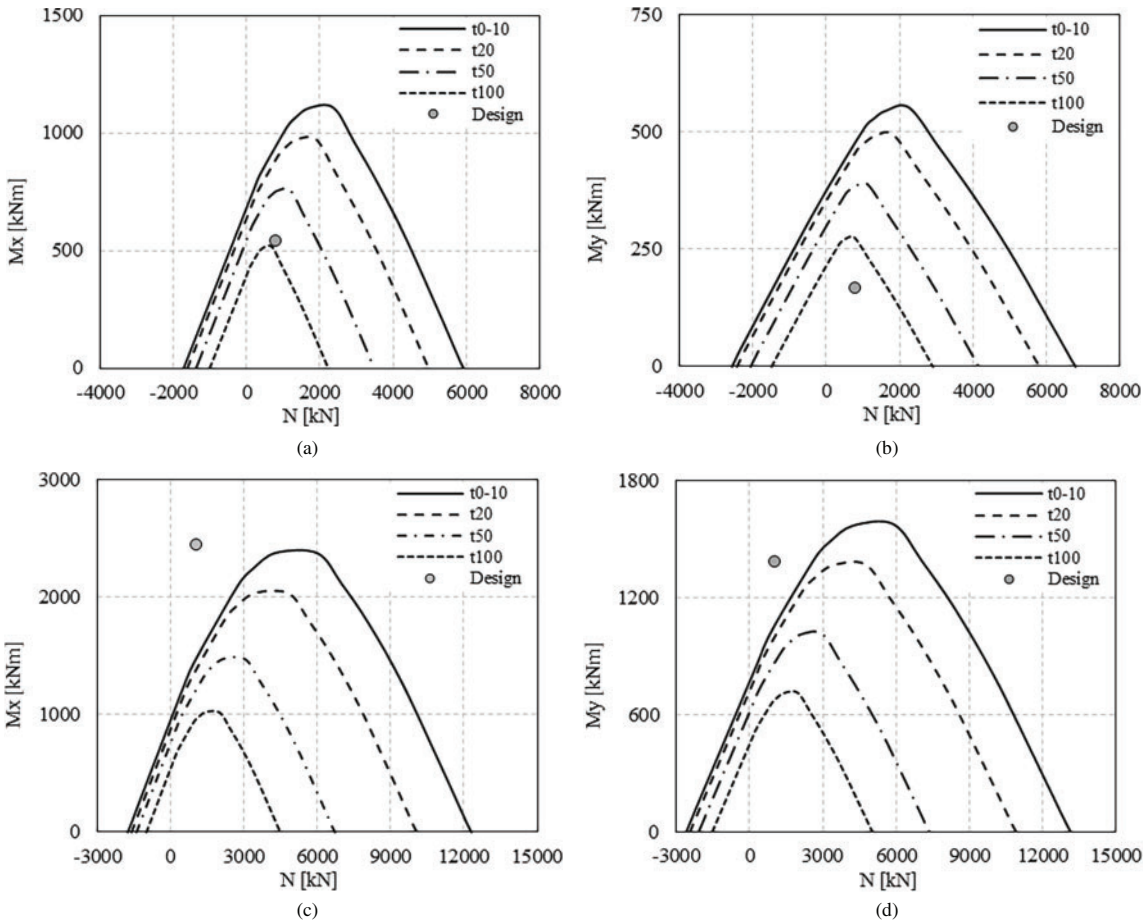

Figure 11. Variation of interaction domain over time: (a) section 85 × 35, x-direction; (b) section 85 × 35, y-direction; (c) section 115 × 65, x-direction; and (d) section 115 × 65, y-direction

previously generated (Fig. 4), were employed. In each analysis, an input set was applied to the bridge's base. The results were then combined to determine the maximum bridge response as specified in the Italian technical standards (NTC[9]). In particular, the hysteresis loops were idealized using an approximated moment–curvature curve to simplify the complex cyclic behavior into a more manageable model for structural analysis. To this end, the envelope curve was derived from the maximum points of the cycles, then the yield point was identified, and lines representing the elastic and plastic segments were drawn adopting the area-equivalence method. Although this approximation results in some loss of information regarding the loading and unloading cycles, it is considered acceptable for the intended evaluations.

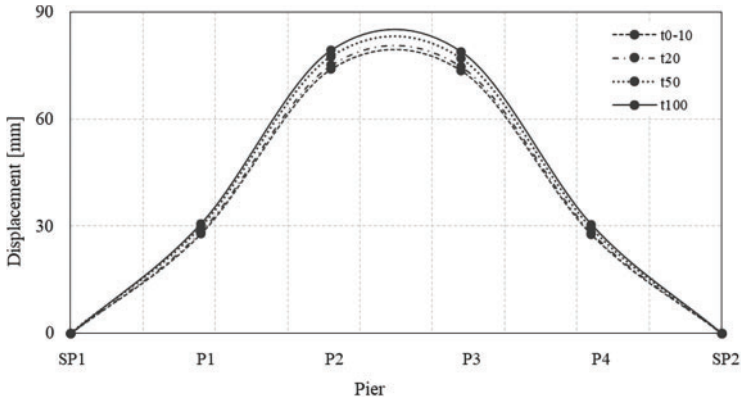

Figure 12. Variation of the transverse displacement at the pier tops over time

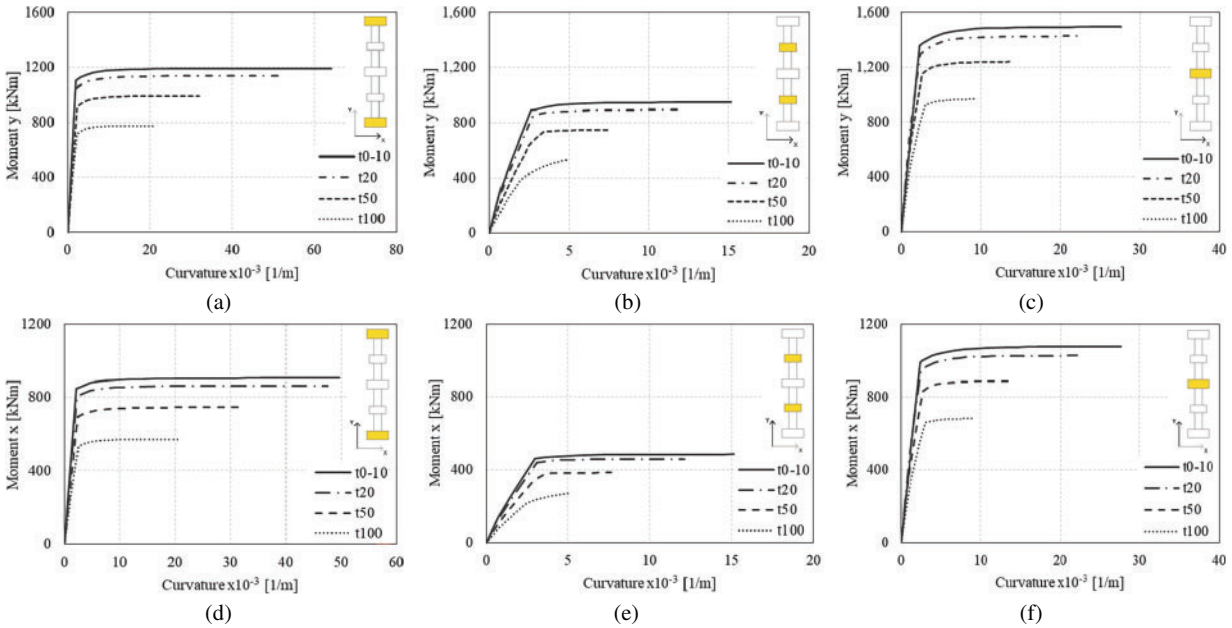

Figure 13. Variation of moment–curvature diagram over time: (a) pier shafts 1–5, *y*-direction; (b) pier shafts 2–4, *y*-direction; (c) pier shaft 3, *y*-direction; (d) pier shafts 1–5, *x*-direction; (e) pier shafts 2–4, *x*-direction; and (f) pier shaft 3, *x*-direction

Fig. 13 shows the moment–curvature relationship for the shafts of the most heavily loaded pier at four significant time intervals (0–10, 20, 50, and 100 years), accounting for the effects of corrosion. From the numerical analysis, the moment–curvature relationship was obtained at the section level. In the nonlinear dynamic analysis, the data take on a cyclic form: at each deformation increment, hysteresis loops were generated, revealing the progressive degradation of stiffness and strength. From these loops, backbone curves were extrapolated enveloping the peak response points for each ascending branch (loading in one direction). The corresponding bilinear curves were then constructed to preserve the main characteristics of the actual response, namely, the initial stiffness, the yield moment, and the ultimate moment.

The diagrams are arranged in two rows: the top row (Fig. 13a–13c) represents the flexural response about the *y*-axis, while the bottom row (Fig. 13d–13f) shows the response about the *x*-axis. The graphs are also grouped into columns, each corresponding to one or more pier shafts: the first column (Fig. 13a, 13d) refers to shafts 1 and 5, the second column (Fig. 13b, 13e) to shafts 2 and 4, while the third column (Fig. 13c, 13f) to shaft 3 of the pier. This grouping is adopted because the bridge is symmetrical in both geometry and applied loading. The graphs clearly show that resistance decreases significantly with increasing corrosion. Ductility and consequently energy dissipation capacity of the section are also markedly reduced. In particular, for shafts 2 and 4 in both directions, corrosion leads to a transition from a ductile to a nearly brittle failure at around 100 years.

The reduction in plastic rotational capacity and ductility has direct consequences on the seismic response of the bridge. The *x*-direction generally exhibits higher resisting moments than the *y*-direction, consistent with greater stiffness and capacity in that direction. Table 5 reports the variation in section ductility (μ_ϕ) and the corresponding

Table 5. Reduction of section ductility over time

	Direction x						Direction y					
	Pier shafts 1–5		Pier shafts 2–4		Pier shaft 3		Pier shafts 1–5		Pier shafts 2–4		Pier shaft 3	
Time	μ_ϕ	$\Delta\mu_{\phi(\%)}$	μ_ϕ	$\Delta\mu_{\phi\ (\%)}$	μ_ϕ	$\Delta\mu_{\phi\ (\%)}$	μ_ϕ	$\Delta\mu_{\phi\ (\%)}$	μ_ϕ	$\Delta\mu_{\phi\ (\%)}$	μ_ϕ	$\Delta\mu_{\phi\ (\%)}$
0–10	29	0	5.4	0	11.1	0	21	0	4.8	0	10.7	0
20	22.4	23	4.2	22	8.6	23	19.7	6	3.8	22	8.2	23
50	13	55	2.2	59	4.9	56	12.5	40	2.1	57	4.8	55
100	8.2	72	1.5	73	3	74	7.8	63	1.4	70	2.9	73

percentage reduction with respect to the undamaged configuration for each pier shaft in both principal directions (x and y). In all configurations, a marked reduction in ductility is observed as corrosion advances.

Conclusions

While the most advanced guidelines for multi-risk assessment of existing bridges emphasize the importance of accounting for degradation to enable realistic safety evaluations, they do not explicitly provide a method for incorporating such degradation, especially corrosion, into seismic vulnerability assessments of reinforced concrete structures through numerical simulations. For this reason, the present work aimed to analyze feasible strategies for explicitly modelling corrosion of relevant infrastructures, to provide a more reliable assessment. To this end, an ordinary reinforced concrete bridge located on a main road of the Italian national route network, constructed between 1961 and 1980, was selected as a significant case study. Both linear and nonlinear dynamic analyses were carried out.

The results indicate that the bridge is structurally inadequate. Moreover, the strengthening intervention applied to the piers proved counterproductive, as it caused a redistribution of the loads with an increase of demand for the jacketed shafts. As degradation advances, there is a clear decline in the ability to withstand applied loads. In the absence of repair interventions, the safety factor continues to decrease over time. This is accompanied by reduced ductility, increased deformability, and decreased energy dissipation capacity. These trends become critical even in the early stages of corrosion and at time intervals comparable to the current age of the bridge, underscoring the importance of incorporating time-dependent degradation effects to accurately assess structural capacity and estimate residual service life.

The modelling strategies adopted proved effective in integrating the effects of corrosion into seismic vulnerability assessment methods commonly used in professional practice, particularly linear dynamic analysis. Moreover, the advanced nonlinear dynamic analyses enabled the quantification of reductions in ductility and energy dissipation capacity, while also revealing changes in collapse mechanisms as degradation progresses.

However, some aspects have emerged that require further investigation. Critical effects of corrosion, such as the reduction in ultimate displacement and the deterioration of the bond between steel and concrete, were not included in the numerical simulations. Another key area for future research is the validation of the model using real-world data. Since this study is based on hypothetical scenarios, the integration of structural monitoring data and the acquisition of a higher level of knowledge about the structure are essential to confirm the reliability of the model in replicating and predicting the behavior of the system under real conditions.

Acknowledgments

This study was supported by FABRE—"Research consortium for the evaluation and monitoring of bridges, viaducts and other structures" (www.consorziofabre.it/en). Any opinion expressed in the paper does not necessarily reflect the view of the funder.

Data Availability Statement

Data reported and discussed in this work are available upon request.

References

[1] Biondini F, Frangopol DM. Life-cycle reliability, risk and performance-based design and assessment of structures and infrastructures. *Struct Infrast Eng*. 2010;6(1–2):1–2.

[2] Frangopol DM, Liu M. Maintenance and life-cycle management of civil infrastructure based on condition, safety, optimisation, and life-cycle cost. *Struct Infrast Eng*. 2007;3(1):29–41.

[3] American Society of Civil Engineers. Bridges: 2025 Infrastructure Report Card; 2025. https://www.infrastructurereportcard.org/wp-content/uploads/2025/03/Full-Report-2025-Natl-IRC-WEB.pdf

[4] Omar T, Nehdi ML. Condition assessment of reinforced concrete bridges: current practice and research challenges. *Infrastructures*. 2018;3(3):36. doi:10.3390/infrastructures3030036.

[5] Zizi M, Bencivenga P, De Matteis G. Handling policies for Italian existing bridges with a territorial approach: the case

study of Caserta, Italy. *Structures*. 2023;48(2023):1306–1321. doi:10.1016/j.istruc.2022.12.114.

[6] Calvi GM, Moratti M, O'Reilly GJ, et al. Once upon a Time in Italy: the tale of the morandi bridge. *Struct Eng Int*. 2019;29(2):198–217. doi:10.1080/10168664.2018.1558033.

[7] Malomo D, Scattareggia N, Orgnoni A, et al. Numerical study of the collapse of the Morandi bridge. *J Perform Constr Facil*. 2020;34(4). doi:10.1061/(asce)cf.1943-5509.0001428.

[8] Salvatore W, Uva G, Venanzi I, et al. Application of Italian Guidelines for structural-foundational and seismic risk classification of bridges: The Fabre experience on a large bridge inventory. *Procedia Struct Integ*. 2024;62:1–8. doi:10.1016/j.prostr.2024.09.009.

[9] NTC 2018. Decree 17/01/2018, n. 42. https://www.gazzettaufficiale.it/eli/id/2018/2/20/18A00716/sg

[10] EN 1998-2:2005. Eurocode 8: Design of structures for earthquake resistance-Part 2: Bridges. https://eurocodes.jrc.ec.europa.eu/EN-Eurocodes/eurocode-8-design-structures-earthquake-resistance

[11] Grieco LA, Scattarreggia N, Monteiro R, Parisi F. An index-based multi-hazard risk assessment method for prioritisation of existing bridge portfolios. *Int J Disaster Risk Reduct*. 2024;114(2):104895. doi:10.1016/j.ijdrr.2024.104895.

[12] Saler E, Donà M, Pernechele V, Tecchio G, da Porto F. Characterisation of an urban bridge portfolio and multi-risk prioritisation accounting for deterioration and seismic vulnerability. *Int J Disaster Risk Reduct*. 2022;87(8):103596. doi:10.1016/j.ijdrr.2023.103596.

[13] Masciotta MG, Barontini A, Chaves E, Mendes N, Brando G, Lourenço PB. Modal-based multi-criteria optimization of sensor placement techniques for dynamic monitoring of bridges. *Int J Bridge Eng, Manag Res*. 2025;2(2):214250017.

[14] Barontini A, Perera R, Masciotta MG, Amado-Mendes P, Ramos L, Lourenço P. Deterministically generated negative selection algorithm for damage detection in civil engineering systems. *Eng Struct*. 2019;197:109444.

[15] García-Macías E, Hernández-González IA, Ubertini F. Incorporating digital twins and artificial intelligence for next-generation SHM software. In: *International Operational Modal Analysis Conference*; May 2024; Cham: Springer Nature Switzerland. p. 435–447.

[16] Ministero delle Infrastrutture e della Mobilità Sostenibili–CSLLPP. Linee guida per la classificazione e gestione del rischio, la valutazione della sicurezza ed il monitoraggio dei ponti esistenti. Decreto Ministeriale n. 204 del 1° luglio 2022. 2022. https://www.mit.gov.it/normativa/decreto-ministeriale-numero-204-del-1-luglio-2022

[17] ANSFISA. Istruzioni Operative per L'applicazione delle Linee Guida per la Classificazione e Gestione del Rischio, la Valutazione della Sicurezza ed il Monitoraggio dei Ponti Esistenti. 2022. https://www.ansfisa.gov.it/linee-guida2

[18] MIT, Ministero delle Infrastrutture e dei Trasporti. Linee Guida per la Classificazione e Gestione del Rischio, la Valutazione della Sicurezza ed il Monitoraggio dei Ponti Esistenti. 2020. https://www.mit.gov.it/normativa/decreto-ministeriale-numero-578-del-17122020

[19] Buttarazzi F, Chiaia B, Marano GC, Palmisano F. Assessment of existing bridges: difficulties and challenges following the Italian experience. *ce/papers*. 2023;6(5):198–204. doi:10.1002/cepa.2180.

[20] Santarsiero G, Masi A, Picciano V, Digrisolo A. The Italian guidelines on risk classification and management of bridges: applications and remarks on large scale risk assessments. *Infrastructures*. 2021;6(8):111. doi:10.3390/infrastructures6080111.

[21] Rossi PP, Spinella N, Recupero A. Experimental application of the Italian guidelines for the risk classification and management and for the safety evaluation of existing bridges. *Structures*. 2023;58(2):105387. doi:10.1016/j.istruc.2023.105387.

[22] Andrade C, Alonso C. Corrosion rate monitoring in the laboratory and on-site. *Const Build Mat*. 1996;10(5):315–328.

[23] Vu KAT, Stewart MG. Structural reliability of concrete bridges including improved chloride-induced corrosion models. *Struct Safety*. 2000;22(4):313–333.

[24] Cui F, Zhang H, Ghosn M, Xu Y. Seismic fragility analysis of deteriorating RC bridge substructures subject to marine chloride-induced corrosion. *Eng Struct*. 2018;155(1):61–72. doi:10.1016/j.engstruct.2017.10.067.

[25] Ma W, Ma S, Chen S. Experimental and simulation study on seismic resilience in bridge piers affected by saline soil corrosion. *Eng Struct*. 2025;330:119900. doi:10.1016/j.engstruct.2025.119900.

[26] Afsar Dizaj E, Salami MR, Kashani MM. Seismic vulnerability analysis of irregular multi-span concrete bridges with different corrosion damage scenarios. *Soil Dynam Earthquake Eng*. 2023;165(6):107678. doi:10.1016/j.soildyn.2022.107678.

[27] Almusallam AA. Effect of degree of corrosion on the properties of reinforcing steel bars. *Construct Build Mater*. 2001;15(8):361–368. doi:10.1016/s0950-0618(01)00009-5.

[28] Idhamou L, Mansouri M, Lakhouili A. Evaluation of corrosion initiation time for reinforced concrete rebars. *Mat Today: Proc*. 2024. doi:10.1016/j.matpr.2024.02.026.

[29] Di Carlo F, Meda A, Rinaldi Z. Numerical evaluation of the corrosion influence on the cyclic behaviour of RC columns. *Eng Struct*. 2017;153(4):264–278. doi:10.1016/j.engstruct.2017.10.020.

[30] Pinto F, Astroza R, Bazáez R, Hernandez F, Navarro N. Probabilistic seismic assessment of multispan RC highway bridges considering soil-structure interaction and chloride-induced corrosion. *Eng Struct*. 2024;301:117257. doi:10.1016/j.engstruct.2023.117257.

[31] Borzi B, Ceresa P, Franchin P, Noto F, Calvi GM, Pinto PE. Seismic vulnerability of the Italian roadway bridge stock. *Earthq Spectra*. 2015;31(4):2137–2161. doi:10.1193/070413eqs190m.

[32] Nielson BG, DesRoches R. Analytical seismic fragility curves for typical bridges in the central and southeastern United States. *Earthq Spectra*. 2007;23(3):615–633. doi:10.1193/1.2756815.

[33] Lei X, Sun L, Xia Y. Seismic fragility assessment and maintenance management on regional bridges using bayesian multi-parameter estimation. *Bullet Earthquake Eng*. 2021;19(15):6693–6717.

[34] Moschonas IF, Kappos AJ, Panetsos P, Papadopoulos V, Makarios T, Thanopoulos P. Seismic fragility curves for greek bridges: methodology and case studies. *Bull Earthq Eng*. 2009;7(2):439–468. doi:10.1007/s10518-008-9077-2.

[35] Avsar O, Yakut A, Caner A. Analytical fragility curves for ordinary highway bridges in Turkey. *Earthq Spectra*. 2011;27(4):971–996. doi:10.1193/1.3651349.

[36] Perdomo C, Monteiro R, Sucuoglu ˘ H. Development of fragility curves for singlecolumn RC italian bridges using nonlinear static analysis. *J Earthq Eng*. 2022;26(5):2328–2352. doi:10.1080/13632469.2020.1760153.

[37] Crespi P, Scamardo M, Buoninconti R. Fragility curves for the seismic vulnerability of a stock of Italian highway bridges. *Structures*. 2025;78:109374. doi:10.1016/j.istruc.2025.109374.

[38] Zhang W, Liu Y, Yu Q-Q. Time-dependent seismic fragility analysis of reinforced concrete columns subjected to chloride-induced corrosion. *Eng Struct*. 2024;302:117448.
[39] Vishwanath BS, Banerjee S. Considering uncertainty in corrosion process to estimate life-cycle seismic vulnerability and risk of aging bridge piers. *Reliab Eng Syst Safety*. 2023;232:109050.
[40] Wang T, Hu M, Jia X, Bi K, Han Q, Du X. Time-varying seismic fragility and risk analysis of precast concrete bridges under the coupling of chloride corrosion and freeze-thaw cycles. *Eng Struct*. 2025;335(3):120413. doi:10.1016/j.engstruct.2025.120413.
[41] Dong Y, Frangopol DM, Saydam D. Time-variant sustainability assessment of seismically vulnerable bridges subjected to multiple hazards. *Earthquake Eng Struct Dynamics*. 2013;42(10):1451–1467. doi:10.1002/eqe.2281.
[42] Zhong J, Mao Y, Yuan X. Lifetime seismic risk assessment of bridges with construction and aging considerations. *Structures*. January 2023;47:2259–2272.
[43] Domaneschi M, De Gaetano A, Casas JR, Cimellaro GP. Deteriorated seismic capacity assessment of reinforced concrete bridge piers in corrosive environment. *Struct Conc*. 2020;1–16. doi:10.1002/suco.202000106.
[44] Akiyama M, Frangopol DM, Matsuzaki H. Life-cycle reliability of RC bridge piers under seismic and airborne chloride hazards. *Earthq Eng Struct Dyn*. 2011;40(15):1671–1687. doi:10.1002/eqe.1108.
[45] Akiyama M, Frangopol DM. Long-term seismic performance of RC structures in an aggressive environment: emphasis on bridge piers. *Struct Infrastruct Eng*. 2014;10(7):865–879. doi:10.1080/15732479.2012.761246.
[46] Crespi P, Zucca M, Valente M, Longarini N. Influence of corrosion effects on the seismic capacity of existing RC bridges. *Eng Fail Anal*. 2022;140(12):106546. doi:10.1016/j.engfailanal.2022.106546.
[47] Hussain RR, Ishida T. Critical carbonation depth for initiation of steel corrosion in fully carbonated concrete and development of electrochemical carbonation induced corrosion model. *Int J Electrochem Sci*. 2009;4(8):1178–1195. doi:10.1016/s1452-3981(23)15216-3.
[48] Imperatore S, Rinaldi Z, Drago C. Degradation relationships for the mechanical properties of corroded steel rebars. *Construct Build Mat*. 2017;148(2017):219–230. doi:10.1016/j.conbuildmat.2017.04.209.
[49] Coronelli D, Gambarova P. Structural assessment of corroded reinforced concrete beams: modeling guidelines. *J Struct Eng, ASCE*. 2004;130(8):1214–1224. doi:10.1061/(asce)0733-9445(2004)130:8(1214).
[50] Meda A, Mostosi S, Rinaldi Z, Riva P. Experimental evaluation of the corrosion influence on the cyclic behaviour of RC columns. *Eng Struct*. 2014;76:112–123.
[51] Guo A, Li H, Ba X, Guan X, Li H. Experimental investigation on the cyclic performance of reinforced concrete piers with chloride-induced corrosion in marine environment. *Eng Struct*. 2015;105:1–11. doi:10.1016/j.engstruct.2015.09.031.
[52] Yang SY, Song XB, Jia HX, Chen X, Liu XL. Experimental research on hysteretic behaviors of corroded reinforced concrete columns with different maximum amounts of corrosion of rebar. *Construct Build Mat*. 2016;121(8):319–327. doi:10.1016/j.conbuildmat.2016.06.002.
[53] Xu G, Feng D, Wu G, Cotsovos DM, Lu Y. Analytical modeling of corroded RC columns considering flexure-shear interaction for seismic performance assessment. *Bullet Earthquake Eng*. 2020;18:2165–2190.
[54] Di Mucci VM, Cardellicchio A, Nettis A, Ruggieri S, Renò V, Uva G. Cv-based corrosion classification to improve fast seismic assessment of existing rc bridge piers. *Eccomas Proceedia COMPDYN*. 2025:1482–1492. doi:10.7712/120125.12504.25332.
[55] Di Sarno L, Pugliese F. Numerical evaluation of the seismic performance of existing reinforced concrete buildings with corroded smooth rebars. *Bullet Earthquake Eng*. 2020;18(9):4227–4273. doi:10.1007/s10518-020-00854-8.
[56] The European Union–Brite EuRam II. Modelling of Degradation. Duracrete. Probabilistic performance based durability design of concrete structures. Document BE95-1347/R4-5. December 1998. https://cordis.europa.eu/project/id/BRPR950132
[57] Silva A, Neves R, De Brito J. Statistical modelling of carbonation in reinforced concrete. *Cem Concr Compos*. 2014;50:73–81. doi:10.1016/j.cemconcomp.2013.12.001.
[58] Hills TP, Gordon F, Florin NH, Fennell PS. Statistical analysis of the carbonation rate of concrete. *Cem Concr Res*. 2015;72:98–107. doi:10.1016/j.cemconres.2015.02.007.
[59] Fib Bulletin 34. Model code for service life design. 2006. doi:10.35789/fib.BULL.0034.
[60] Kim Anh TV, Stewart MG. Structural reliability of concrete bridges including improved chloride-induced corrosion models. *Struct Saf.* 2000;22(4):313–333. doi:10.1016/s0167-4730(00)00018-7.
[61] Saetta A, Scotta R, Vitaliani R. Coupled environmental-mechanical damage model of RC structures. *J Eng Mech*. 1999;125(8):930–940. doi:10.1061/(asce)0733-9399(1999)125:8(930).
[62] Wang X, Liu X. Modeling the flexural carrying capacity of corroded RC beam. *J Shanghai Jiaotong Univ (Sci)*. 2008;13(2):129–135. doi:10.1007/s12204-008-0129-1.
[63] Lee HS, Tomosawa F, Noguchi T. Effect of rebar corrosion on the structural performance of singly reinforced beams. In: Sjostrom C. (Ed.), *Durability of Building Materials and Components*. Vol. 7. London: E and FN Spon; 1996:571–558.
[64] Morinaga S. Remaining life of reinforced concrete structures after corrosion cracking. In: Sjostrom C. (Ed.), *Durability of Building Materials and Components*. London: E and FN Spon; 1996:127–137.
[65] Zhang PS, Lu M, Li X. The mechanical behaviour of corroded bar. *J Ind Build*. 1995;25(257):41–44.
[66] Clark LA, Saifullah M. Effect of corrosion rate on the bond strength of corroded reinforcement. In: Swamy RN. (Eds.), *Corrosion and Corrosion Protection of Steel in Concrete*. Sheffield: Sheffield Academic Press; 1994:591–602 doi:10.1016/0958-9465(95)90016-0.
[67] Ghanooni-Bagha M, Shayanfar MA, Shirzadi-Javid AA, Ziaadiny H. Corrosion induced reduction in compressive strength of self-compacting concrete containing mineral admixtures. *Construct Build Mat*. 2016;113(2016):221–228. doi:10.1016/j.conbuildmat.2016.03.046.
[68] Imperatore S, Rinaldi Z, Spagnulo S. Experimental investigations on the effects of the steel rebar corrosion at structural level. *Structural Concrete*. 2019;1–12. doi:10.1002/suco.201900246.
[69] Molina FJ, Alonso C, Andrade C. Cover cracking as a function of rebar corrosion: Part 2-Numerical model. *Mat Struct*. 1993;26(9):532–548. doi:10.1007/bf02472864.
[70] Midas Civil. Integrated solution system for bridge and civil engineering. 2024. https://www.cspfea.net/doc_prodotti/Midas-Civil/cspfea-midas-civil-scheda-tecnica.pdf

[71] Park R, Priestley MJN, Gill WD. Ductility of square-confined concrete columns. *J Struct Div, ASCE*. 1982;108(4):929–950.
[72] Menegotto M, Pinto PE. Method of analysis for cyclically loaded reinforced concrete plane frames including changes in geometry and non-elastic behaviour of elements under combined normal force and bending. *IABSE Symposium of Resistance and Ultimate Deformability of Structures Acted on by Well-defined Repeated Loads*. Lisbon, Portugal: International Association of Bridge and Structural Engineering; 1973;13:15–22.
[73] Taucer FF, Spacone E, Filippou FC. A fiber beam-column element for seismic response analysis of reinforced concrete structures. Report No. UCB/EERC-91/17 Earthquake Engineering Research Center, College of Engineering University of California, Berkeley. https://nisee.berkeley.edu/elibrary/Text/237794
[74] Fellitti M, Oliveto F, Pelle D, Valvona F. Valutazione di ponti e viadotti esistenti soggetti a rischio strutturale in condizioni statiche, sismiche e di degrado. 978-88-916-6615-4. 2023. https://www.maggiolieditore.it/valutazione-di-ponti-e-viadotti-esistenti-soggetti-a-rischio-strutturale-in-condizioni-statiche-sismiche-e-di-degrado.html